

Structural basis for recruitment of CBP/p300 by hypoxia-inducible factor-1 α

Steven J. Freedman^{*†‡}, Zhen-Yu J. Sun[†], Florence Poy[‡], Andrew L. Kung[‡], David M. Livingston[‡], Gerhard Wagner[†], and Michael J. Eck^{†§}

^{*}Division of Hematology/Oncology, Beth Israel Deaconess Medical Center, 330 Brookline Avenue, Boston, MA 02215; [†]Department of Biological Chemistry and Molecular Pharmacology, 240 Longwood Avenue, Harvard Medical School, Boston, MA 02115; and [‡]Department of Cancer Biology, Dana-Farber Cancer Institute, 44 Binney Street, Boston, MA 02115

Contributed by David M. Livingston, February 28, 2002

Adaptation to hypoxia is mediated by transactivation of hypoxia-responsive genes by hypoxia-inducible factor-1 (HIF-1) in complex with the CBP and p300 transcriptional coactivators. We report the solution structure of the cysteine/histidine-rich 1 (CH1) domain of p300 bound to the C-terminal transactivation domain of HIF-1 α . CH1 has a triangular geometry composed of four α -helices with three intervening Zn²⁺-coordinating centers. CH1 serves as a scaffold for folding of the HIF-1 α C-terminal transactivation domain, which forms a vise-like clamp on the CH1 domain that is stabilized by extensive hydrophobic and polar interactions. The structure reveals the mechanism of specific recognition of p300 by HIF-1 α , and shows how HIF-1 α transactivation is regulated by asparagine hydroxylation.

Hypoxia-inducible factor-1 (HIF-1) is a heterodimeric transcription factor that plays a central role in development and in adaptation to hypoxia by directing the expression of genes that promote angiogenesis, erythropoiesis, and vasodilation (1). The importance of HIF-1 in mammalian development is underscored by the finding that its absence is lethal during embryogenesis, in part because of defective vascularization (2). HIF-1 activation can have adaptive or maladaptive roles in a variety of pathological conditions. For example, HIF-1 allows revascularization after cardiac and cerebral ischemia, but it also allows tumor growth in hypoxic environments by promoting angiogenesis and metabolic adaptations to hypoxia (3).

HIF-1 activity is tightly regulated by oxygen-dependent control of the cellular levels of its HIF-1 α subunit. In the well oxygenated state, HIF-1 α is rapidly degraded in a ubiquitin-dependent manner (4). HIF-1 α degradation is mediated by its hydroxylation on Pro-402 and -564; proline-hydroxylation of HIF-1 α allows it to bind the von Hippel-Lindau tumor suppressor protein Pro-564 (pVHL), the recognition component of a multiprotein E3 ubiquitin ligase complex (5–7). The recently identified and characterized prolyl hydroxylase that marks HIF-1 α for degradation is oxygen-dependent (7, 8). Thus, under hypoxic conditions, HIF-1 α is not marked for degradation, and the stable protein dimerizes with constitutively expressed HIF-1 β (also called ARNT) in the nucleus (9). The active HIF-1 heterodimer binds to cognate promoter elements and drives expression of hypoxia-inducible proteins such as vascular endothelial growth factor, erythropoietin, and nitric oxide synthetase.

Activation of HIF-responsive genes requires recruitment of a transcriptional coactivator such as p300, CBP, or SRC-1 (10–15). CBP and p300 are paralogous, multidomain proteins that serve as transcriptional coactivators by binding the transactivation domains of a vast array of transcription factors and by binding components of the general transcriptional apparatus (16). In addition, they have histone acetyltransferase (HAT) activity. Kung *et al.* (15) mapped the interaction between HIF-1 α and p300; they showed that the C-terminal transactivation domain (CTAD) of HIF-1 α binds the CH1 domain of p300 (Fig. 1). HIF-1 α also contains an N-terminal transactivation domain (NTAD) that transactivates less effectively than CTAD alone;

however, NTAD and CTAD together function synergistically (13, 14, 17, 18). CH1 and CH3 are homologous Zn²⁺-binding domains of CBP/p300 containing numerous cysteine and histidine residues (Fig. 1C). The CH2 domain also binds Zn²⁺ but is structurally unrelated to the CH1 and CH3 domains. With few exceptions the CH1 and CH3 domains bind different sets of transcription factors despite their predicted structural similarity. The p53 tumor-suppressor protein binds both CH1 and CH3, but the binding sites for each are different (19, 20). Surprisingly, there is no apparent sequence homology among transactivation regions that bind to the CH1 domain or among those that bind the CH3 domain.

New insight into the regulation of CBP/p300 recruitment by HIF-1 α is based on the observation that hypoxic induction of transactivation can be uncoupled from hypoxic induction of HIF-1 α stability (12–14, 17, 18). Two mechanisms for this additional level of hypoxic regulation have been proposed. First, a region between NTAD and CTAD that inhibits transactivation was recently shown to form part of a binding site for the novel inhibitory factor, FIH-1 (18, 21). According to this model, FIH-1 may dissociate from HIF-1 α during hypoxia and thereby permit transactivation through CTAD. Second, posttranslational modification of residues in CTAD has been proposed to influence binding to CBP/p300. Initial reports attributed this function to the redox state of Cys-800 (13, 14). However, mutational studies suggest that this cysteine makes hydrophobic interactions and show that hypoxic inducibility is maintained even if Cys-800 is mutated to alanine (22, 23). More recently, asparagine hydroxylation has been discovered as a mechanism for oxygen-dependent regulation of HIF-1 α transactivation. Lando *et al.* (24) demonstrated that Asn-803 in HIF-1 α CTAD is hydroxylated only under normoxic conditions, and that the Asn-803-hydroxylated CTAD does not bind or recruit CBP/p300. Under hypoxic conditions, the hydroxylation is abrogated, allowing CTAD to recruit CBP/p300. Thus, this posttranslational modification provides a “back-up” mechanism to render inactive any HIF-1 α protein that may escape degradation during normoxia.

Despite the abundance of functional data identifying interactions between transcription factors and CBP/p300, little structural information is available. Three-dimensional structures of the isolated KIX, I β Id, and CH3 domains of CBP have been determined using NMR methods (25–27), as has the structure of the KID domain of CREB bound to the KIX domain of CBP (27). However, no structural information is available for either

Abbreviations: HIF, hypoxia-inducible factor; CTAD, C-terminal transactivation domain; CH1/2/3, cysteine/histidine-rich domains 1/2/3; NOESY, nuclear Overhauser effect spectroscopy.

Data deposition: The atomic coordinates and structure factors have been deposited in the Protein Data Bank, www.rcsb.org (PDB ID code 1L3E). The NMR chemical shifts have been deposited in the BioMagResBank, www.bmrb.wisc.edu (accession no. 5306).

[§]To whom reprint requests should be addressed. E-mail: eck@red.dfci.harvard.edu.

The publication costs of this article were defrayed in part by page charge payment. This article must therefore be hereby marked “advertisement” in accordance with 18 U.S.C. §1734 solely to indicate this fact.

Table 1. Statistical analysis of 17 CTAD/CH1 Structures

NOE distance restraints, no.	
Intraresidue	306
Medium range (≤ 4)	554
Long range (> 4)	266
Total (intramolecular/intermolecular)	1,126 (1,013/113)
Hydrogen bond restraints, no.	
	94
Backbone dihedral angle restraints (ϕ and ψ), no.	
	158
Ramachandran plot	
Most favored region, %	80.1
Additionally allowed region, %	18.8
Generously allowed region, %	1.0
Disallowed region, %	0.1
Average RMSD from mean structure (backbone)	
CTAD/CH1 complex, Å	0.638
CTAD alone, Å	0.493
CH1 alone, Å	0.632

Seventeen of 25 structures with NOE violations ≤ 0.3 Å or angle violations $< 5^\circ$. Only well defined regions of HIF-1 α (residues 792–824) and p300 (residues 331–407 and 411–418) were analyzed. Results were obtained using MOLMOL (40) and PROCHECK NMR (43). RMSD, rms deviation.

intertwine to form a single structural domain with a common hydrophobic core. Further, the structure shows why hydroxylation of Asn-803 would be expected to destabilize the complex.

Materials and Methods

Protein Expression. A DNA fragment encoding amino acids 786–826 of human HIF-1 α was cloned into the *Bam*H1 and *Eco*R1 sites of a pET vector (Novagen) that was engineered to express a glutathione *S*-transferase (GST) fusion containing a tobacco etch virus (TEV) protease site. A DNA fragment encoding amino acids 323–423 of human p300 was cloned into a compatible pACYC vector that expresses only the free peptide. The two vectors were cotransformed into *Escherichia coli* strain BL21(DE3). Unlabeled or uniformly isotope-labeled protein was obtained with LB broth or M9-minimal media containing 0.1 mM ZnSO₄, ¹⁵NH₄Cl and/or ¹³C₆-glucose (Cambridge Isotope Laboratories, Cambridge, MA). Bacteria were lysed by sonication, and the HIF-1 α CTAD/p300 CH1 complex in the supernatant fraction was isolated on glutathione Sepharose 4B resin (Amersham Pharmacia). The CTAD/CH1 complex was eluted with TEV protease. The complex was $>99\%$ pure, as verified by SDS/PAGE.

NMR Structure Determination. NMR samples with 0.8–1.0 mM CTAD/CH1 peptide complex were prepared in 1 mM DTT/0.1 mM ZnSO₄/100 mM NaCl/10% (vol/vol) D₂O, pH 6.0. Samples in $>99.9\%$ D₂O were obtained by buffer exchange over a PD10 desalting column (Amersham Pharmacia). Stereospecific assignments of valine and leucine methyl groups were made by using a 10% ¹³C-labeled sample (28). The standard NMR methodology was used as described (29). All spectra were acquired at 25°C. The amides for three residues in CH1 (Met-323, Gly-324, His-368) were not assigned, presumably because of high mobility. NMR distance restraints were obtained from a nuclear Overhauser effect spectroscopy (NOESY) spectrum acquired on a Unity-Inova 750 MHz spectrometer (Varian) and a ¹⁵N-NOESY-HSQC spectrum acquired on an Avance 500 MHz spectrometer with a cryogenic probe (Bruker, Billerica, MA). NMR data processing and analysis were carried out with PROSA (30) and XEASY (31).

NMR-derived restraints are shown in Table 1. Stereospecific distance restraints were used for 13 leucines and 6 valines. The backbone dihedral angle restraints were obtained from chemical shift index analysis with the TALOS program (32). H-bond

restraints were incorporated if they were supported by NOE analysis and were protected from H₂O/D₂O exchange for >3 h. Structure calculations by simulated annealing were performed by using X-PLOR (33).

Zn²⁺-binding sites were inferred by the presence of NOEs between the histidine ring and cysteines of each canonical HCCC Zn²⁺-binding sequence and chemical shift analysis of cysteines involved in Zn²⁺ binding. The nine cysteine residues in CH1 have downfield-shifted ¹³C β resonances (28.3–31.1 ppm; avg. 29.7 ppm) consistent with the known effect of Zn²⁺ coordination on this ligand (25). In contrast, the single cysteine in the HIF-1 α CTAD has a ¹³C β chemical shift value (26.8 ppm) characteristic of an unliganded sulfhydryl group. Distance restraints between cysteine S γ and Zn²⁺ (2.35 Å) and histidine N ϵ and Zn²⁺ (2.05 Å) were used for structures calculated with Zn²⁺ atoms (34).

Results and Discussion

Structure Determination. A minimal HIF-1 α /p300 complex was reported to include human p300 residues 302–418 and human HIF-1 α residues 786–826 (15). We identified a slightly smaller region of p300, spanning residues 323–423, which retains full HIF-1 α binding activity. Functional association between HIF-1 α (residues 786–826) and p300 (residues 323–423) was confirmed by using a mammalian two-hybrid transcriptional assay (15). Moreover, this 323–423 fragment was the approximate core generated by limited proteolysis with trypsin using HIF-1 α (residues 786–826) bound to larger p300 fragments (data not shown). To reconstitute the complex for structural studies, we coexpressed the human HIF-1 α CTAD region and human p300 CH1 domain in *E. coli* and purified the Zn²⁺-containing complex (see *Materials and Methods* and Fig. 1). The purified complex failed to crystallize, but preliminary ¹H-¹⁵N-HSQC experiments revealed a well dispersed spectrum (see supporting information, which is published on the PNAS web site, www.pnas.org). The structure was determined by using multidimensional NMR methods; final structures were calculated with a total of 1,378 NMR-derived restraints (Table 1). The well defined regions of the complex include residues 331–418 of p300 and residues 792–824 of HIF-1 α (Fig. 1*d*).

Overall Structure. The p300 CH1 domain is composed of four α -helices and three Zn²⁺-coordination sites formed by HCCC sequence motifs (Fig. 1). The three longer helices (designated $\alpha 1$, $\alpha 2$, and $\alpha 3$) pack across each other to form a roughly triangular structure. The three Zn²⁺ sites lie at the vertices of this triangle, and the coordinating histidine and cysteine residues that compose the HCCC motif are found near the ends of the helices and in the intervening turns. The short C-terminal helix, $\alpha 4$, completes the third Zn²⁺-coordination site and packs against $\alpha 1$ in a parallel fashion. The fold of the CH1 domain is stabilized in part by Zn²⁺ binding; addition of EDTA disrupts the HIF-1 α /p300 complex and yields a ¹H-¹⁵N-HSQC spectrum characteristic of an unfolded protein (see supporting information, which is published on the PNAS web site). The CH1 fold also is stabilized by a single hydrophobic core formed by all four helices (Fig. 1*c*). Importantly, the unusual open packing arrangement of helices $\alpha 1$, $\alpha 2$, and $\alpha 3$ exposes large areas of the hydrophobic core. These exposed hydrophobic regions lie on either side of the domain and largely form the recognition surface for the bound HIF-1 α CTAD. Consequently, CTAD encircles the CH1 domain like a clamp. As described below, the CH1 and CTAD regions share a common hydrophobic core and together form a single structural domain.

HIF-1 α Structure and Recognition. The HIF-1 α CTAD includes four structural elements: an N-terminal extended region, two helices, αA and αB , and an intervening loop (Fig. 1*d* and *e*). Interestingly, both the extended N-terminal segment and the C-terminal

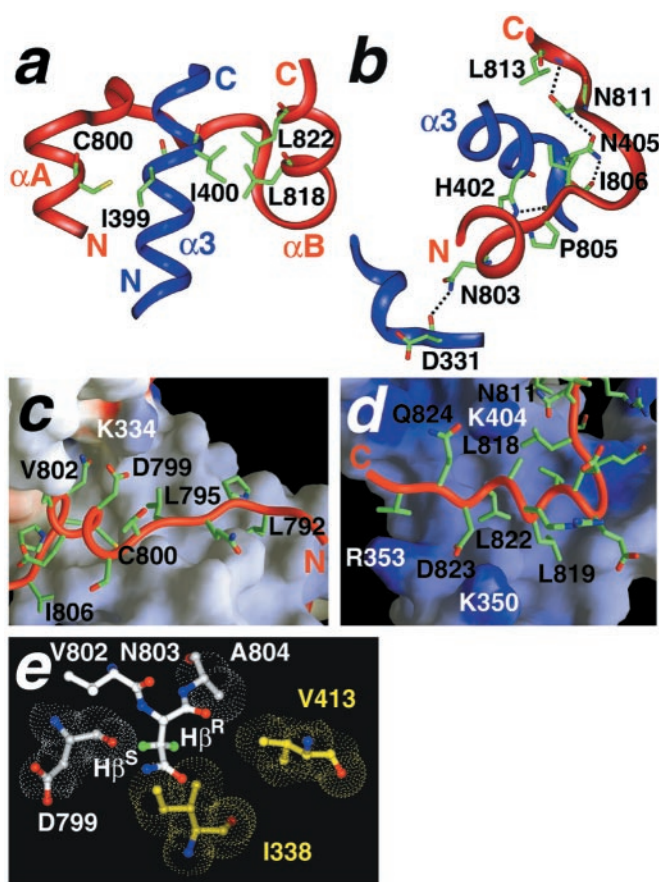


Fig. 2. Intermolecular contacts between the HIF-1 α CTAD and p300 CH1 domains. (a) A region of the CTAD/CH1 complex is magnified to illustrate some of the important hydrophobic contacts that define the topology of the interaction. CTAD wraps around CH1 like a clamp such that α A and α B rest in grooves on either side of α 3. Note the parallel configuration of the CH1 helix sandwiched between the two CTAD helices. Several hydrophobic side chains considered to contribute to the binding energy are displayed as sticks and are labeled by residue and number. (b) A similar region of the complex (interhelical loop of CTAD, N terminus of α 1 and α 3 from CH1) is shown in a different orientation to illustrate putative intermolecular hydrogen bond contacts that stabilize the complex. The presence of hydrogen bonds is supported by NOE and structure analyses. (c and d) The N- and C-terminal regions of the HIF-1 α CTAD (red ribbon) are shown with the p300 CH1 domain represented as an accessible surface. The surface is colored by charge and is scaled from -10 kT/e (red) to $+10$ kT/e (blue). Selected HIF-1 α side chains are labeled in black. Basic residues in CH1 are labeled in white. (e) Position of Asn-803 in the CTAD/CH1 complex indicates how β -hydroxylation would inhibit binding. CH1 residues are shown in yellow and CTAD residues are shown in white. The Asn-803 H β (pro-*R*) and H β (pro-*S*) are colored green. Van der Waals surfaces are shown for residues surrounding the Asn-803 side chain. Substitution of either the pro-*R* or pro-*S* β -protons with a hydroxyl group would disfavor complex formation because of steric and hydrogen-bonding considerations (see text). (a, b, and e) Complexes were prepared with INSIGHTII (Accelrys). (c and d) Complexes were prepared with GRASP (42).

helix α B contact residues in each of the three major helices in CH1 but on opposite sides of the triangular domain. The interhelical loop straddles α 3 in CH1, and α A and α B are buried in grooves on either side of it in a nearly parallel arrangement. Helices α A and α B resemble the jaws of a vise that clamp around α 3 in the CH1 domain.

Each of the four components of the HIF-1 α CTAD makes significant hydrophobic and/or polar interactions with the CH1 domain that contribute to specific recognition (Fig. 2). The N-terminal extended region is anchored by Leu-792 and Leu-

795, which pack into the hydrophobic core with residues Ile-338, Leu-344, Met-372, and Ile-399 in CH1. The α A helix packs in a groove created by the nearly perpendicular intersection of helices α 1 and α 3 in CH1. The hydrophobic side chains of HIF-1 α residues Tyr-798, Cys-800, Val-802, and Ala-804 are all significantly buried in the interface (Figs. 1b and 2a and c). Asp-799 is positioned to make complementary electrostatic interactions with Lys-334 in p300 (Fig. 2c). The interactions of the interhelical loop are mostly polar; for example, an extensive hydrogen-bond network links the carbonyl of Ile-806, the side chain of Asn-811, and the backbone amide of Leu-813 with Asn-405 in the CH1 domain (Fig. 2b). The amphipathic C-terminal helix of the HIF-1 α CTAD packs in the center of the CH1 triangle, approximately parallel to α 3. Leu-818, Leu-819, and Leu-822 contribute to the hydrophobic core of the complex (Figs. 1c, 2a and d). The side chain of Asp-823 extends into a positively charged pocket formed by His-349, Lys-350, and Arg-353 in CH1 (Fig. 2d).

A random mutagenesis screen identified four HIF-1 α residues (Leu-795, Cys-800, Leu-818, and Leu-822) as critical for p300 recruitment (23); the structure reveals that all of these residues are buried in the core of the complex. Likewise, the study identified four p300 residues as critical for interaction with HIF-1 α (residues Leu-344, Leu-345, Cys-388, and Cys-393). The two leucines are found in the HIF-1 α interface, and the two cysteines participate in Zn²⁺ coordination and are, therefore, indirectly required for HIF-1 α binding.

The extensive interactions of the HIF-1 α CTAD and p300 CH1 domain bury a total surface area of 3,393 Å². This buried surface area is more than double the average value of 1,600 \pm 400 Å² for protein-protein recognition sites (35). The tertiary structure of the HIF-1 α CTAD is determined exclusively by intermolecular contacts with CH1; the secondary structure elements of the HIF-1 α CTAD make essentially no contacts with one another (see supporting information, which is published on the PNAS web site). The entire HIF-1 α CTAD domain is literally embedded in the CH1 structure such that almost half of its surface is buried in the interface (Fig. 3a). Furthermore, the HSQC spectrum recorded after pretreatment of the complex with EDTA (see supporting information, which is published on the PNAS web site) shows that in the absence of a folded CH1 domain, HIF-1 α also is unstructured. Thus, we conclude that the Zn²⁺-bound CBP/p300 CH1 domain presents a scaffold onto which the HIF-1 α CTAD can fold, and the two proteins together form a single structural domain.

Regulation of HIF-1 α Recruitment by Hydroxylation of Asn-803. Hydroxylation of Asn-803 during normoxia prevents recruitment of p300 by HIF-1 α (24). The asparagine side chain is hydroxylated on the β -carbon, such that one β -proton is replaced by a hydroxyl group (36). The location of Asn-803 in the interface of our complex is striking. Approximately 45% of its surface is buried in the interface, making it the single most buried HIF-1 α residue in the complex (Fig. 1b). The orientation of the side chain is well defined in our structure; its amide is positioned to make an intermolecular H-bond contact with Asp-331 in p300 (Fig. 2b). The specific enzyme that hydroxylates the HIF-1 α CTAD has not been identified, and the stereochemistry of the modification is not known. However, the present structure shows that hydroxylation in either the pro-*R* or pro-*S* positions would create unfavorable interactions. In the complex, the Asn-803 pro-*R* β -proton is buried in a hydrophobic pocket composed of Ala-804, Ile-338, and Val-413 (Fig. 2e). Substitution of this proton with a hydroxyl group would create a minor steric clash with Ile-338 in the CH1 domain and would also place the hydroxyl group in an energetically unfavorable hydrophobic environment with no hydrogen-bonding partner. Hydroxylation in the pro-*S* position would create a direct steric clash with the backbone

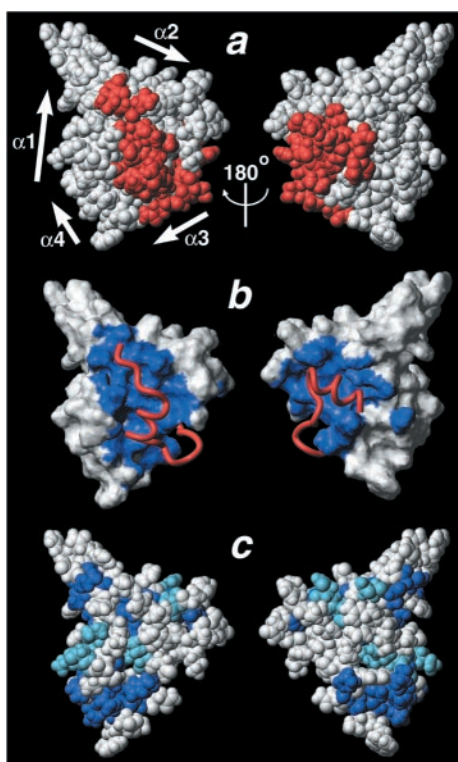


Fig. 3. The HIF-1 α CTAD/p300 CH1 interface. (a–c) The CH1 domain is shown in the same orientation, and the view on the right is rotated $\approx 180^\circ$ about the vertical axis. (a) A space-filling CPK model of the complex. The HIF-1 α CTAD is colored red, and the p300 CH1 domain is shown in white. The HIF-1 α CTAD is embedded in the CH1 scaffold so that the complex appears as a single domain. (b) The surface of the CH1 domain is shown in white with the HIF-1 α CTAD-binding surface shaded blue. The bound HIF-1 α CTAD is shown as a red ribbon. (c) A space-filling model of CH1 in which residues that are identically conserved in human CBP/p300 CH3 are shown in royal blue, and those that are conservatively substituted are shown in light blue. Comparison of *b* and *c* shows that the HIF-1 α -binding surface is not well conserved in the CH3 domain, which binds different transactivation domains. This figure was prepared with MOLMOL (40).

carbonyl of Asp-799 in HIF-1 α (Fig. 2*e*), thereby disrupting helix αA in HIF-1 α . Thus, the structure supports a model in which hydroxylation of Asn-803, in either the pro-*R* or pro-*S* positions, precludes or diminishes recruitment of p300 by the HIF-1 α CTAD.

Comparison with the CH3 (TAZ2) Domain. The CH3 domain of CBP/p300 is structurally homologous to the CH1 domain, but binds distinct activation domain sequences (Fig. 1*a*). Comparison of the HIF-1 α CTAD/p300 CH1 complex with the solution structure of the free CH3 domain from CBP reveals expected similarities as well as unanticipated differences (25). As anticipated, the arrangement of the three major helices is well conserved between CH1 and CH3; 44 C α atoms in helices $\alpha 1$, $\alpha 2$, and $\alpha 3$ of the two structures superimpose with an rms deviation of 1.0 Å (Fig. 1*f*). Although Zn $^{2+}$ -coordinating residues and many residues in the hydrophobic core are conserved between CH1 and CH3 (Fig. 1*c*), the CH1 surface bound by HIF-1 α is not conserved in the CH3 domain (Fig. 3 *b* and *c*). This divergence in the ligand-binding surface is one obvious basis for binding specificity. Additionally, we unexpectedly find that the position of helix $\alpha 4$ and the third Zn $^{2+}$ -coordination site differs dramatically in the CH3 domain (Fig. 1*f*). In the isolated CH3 structure, helix $\alpha 4$ is rotated nearly 180° and shifted by ≈ 14 Å relative to its position in the CH1 complex. Consequently, the position of

the third Zn $^{2+}$ coordination site differs by ≈ 8 Å relative to its location in the CH1 complex. This arrangement of helix $\alpha 4$ and the adjacent Zn $^{2+}$ site in CH3 largely overlaps the space occupied by the C-terminal portion of the HIF-1 α peptide in the CH1 complex (Fig. 1 *e* and *f*). Structural studies of unbound CH1 will need to be done to clarify whether this conformational difference confers specificity of HIF-1 α CTAD binding to CH1 or whether it represents a CTAD-induced conformational change.

Implications for Inhibitor Development. Tumors survive and grow in their hypoxic environments as a result of a number of adaptive mechanisms mediated by HIF-1 α , including angiogenesis, vasodilation, and anaerobic metabolism. Thus, preventing or terminating HIF-1 α transactivation has the potential to interfere with tumor growth. In validation of this concept, a recent study demonstrated that peptide inhibitors of the HIF-1 α /p300 interaction caused suppression of tumor growth *in vivo* (15). The remarkably extensive interaction between HIF-1 α and p300 revealed by the present structure suggests that development of small molecule transcriptional modulators targeting this complex will present a considerable challenge. However, if lead compounds can be identified by screening compound libraries, then p300/HIF-1 α structure will provide a valuable resource for optimizing and refining inhibitors.

CH1: A Versatile Binding Scaffold. In addition to HIF-1 α , a number of other transcription factor activation domains, including p53, STAT2, Pit-1, and Ets-1, have been shown to bind the CH1 region of p300. Although these activation domains share little recognizable sequence similarity with HIF-1 α or with each other, we expect that they will fold on the CH1 scaffold and complement its hydrophobic core in a manner roughly analogous to that observed in the HIF-1 α /p300 complex. Examination of the surface of CH1, colored by electrostatic potential, reveals that the hydrophobic-binding regions are flanked by areas of positive charge (Fig. 2 *c* and *d*). Like HIF-1 α , other binding partners also are likely to make complementary interactions with these basic residues, as most transcription factor activation domains carry a net negative charge.

Given that the diverse activation domains that bind the CH1 domain share little recognizable sequence similarity with HIF-1 α or with each other, how are they recognized with high affinity by the CH1 domain? The eclectic binding repertoire of the CH1 domain likely stems from the nature of the CH1 scaffold and the use of induced folding as a binding mechanism. The extensive binding interface and multisite nature of the interaction may allow considerable variation in binding sequences because substitutions that diminish the affinity at one site might be compensated by substitutions that increase affinity at a second site. Additionally, a subset of the hydrophobic binding clefts in CH1 may allow substantial sequence variation. For example, substitution of Cys-800 in HIF-1 α with alanine or valine preserves p300 binding but hydrophilic substitutions do not (23). Further sequence diversity may arise from the possibility of insertions or deletions between binding elements of cognate-activation domains. For example, examination of the HIF-1 α complex suggests that it may tolerate small insertions or deletions in the loop linking αA and αB . It is also possible that some activation domains will bind in a structurally divergent manner that still complements the CH1 fold. There is precedent for such a mechanism; a recent comparison of β -catenin in complex with Tcf-3 and E-cadherin revealed a region in which two leucine residues in an extended conformation in E-cadherin “mimic” the binding interactions of leucines in an amphipathic helix in Tcf-3 (37).

Induced folding may be a common mechanism of recognition in transcriptional regulation (38). Comparison of the HIF-1 α /

p300 complex with the structure of the KIX domain of CBP in complex with the phosphorylated KID-activation domain of CREB reveals interesting structural parallels (27). Although the KIX domain is structurally unrelated to the CH1 domain, its CREB-binding partner also contains two amphipathic helices whose folding is induced by complex formation. Additionally, acidic residues (including a phosphorylated serine) make complementary electrostatic interactions with basic residues in the KIX domain. However, the interaction of CREB with the KIX domain is much less extensive; only $\approx 1,200 \text{ \AA}^2$ of surface area are buried, and complex formation does not involve the hydrophobic core of the KIX domain. Very recently, Demarest *et al.* (39) described the “mutual synergistic folding” of a C-terminal domain of CBP with its binding domain in the p160 nuclear-receptor coactivator (a coactivator for the thyroid hormone and

retinoid receptors). These domains are unstructured in isolation but fold together to form a single-domain complex. Although we expect that other activation domains will undergo induced folding upon binding to the CH1 domain, it is clear that a predictive understanding of CH1-recognition properties will require structure analysis of additional transactivation domain complexes.

We thank S. Blacklow, C. North, X. Huang, and A. Rigby for advice and preliminary evaluation of the CH1 protein. This work was supported by grants from the Dana–Farber Cancer Institute/Novartis Drug Discovery Program (to M.J.E., D.M.L., and A.L.K.) and by National Science Foundation Grant MCB 9316938 (to G.W.). S.J.F. is a recipient of a National Institutes of Health K08 award from the National Heart, Lung, and Blood Institute.

- Semenza, G. L. (1999) *Annu. Rev. Cell Dev. Biol.* **15**, 551–578.
- Iyer, N. V., Kotch, L. E., Agani, F., Leung, S. W., Laughner, E., Wenger, R. H., Gassmann, M., Gearhart, J. D., Lawler, A. M., Yu, A. Y., *et al.* (1998) *Genes Dev.* **12**, 149–162.
- Semenza, G. L. (2001) *Trends Mol. Med.* **7**, 345–350.
- Salceda, S. & Caro, J. (1997) *J. Biol. Chem.* **272**, 22642–22647.
- Ivan, M., Kondo, K., Yang, H., Kim, W., Valiando, J., Ohh, M., Salic, A., Asara, J. M., Lane, W. S. & Kaelin, W. G., Jr. (2001) *Science* **292**, 464–468.
- Jaakkola, P., Mole, D. R., Tian, Y. M., Wilson, M. I., Gielbert, J., Gaskell, S. J., Kriegsheim, A., Hebestreit, H. F., Mukherji, M., Schofield, C. J., *et al.* (2001) *Science* **292**, 468–472.
- Epstein, A. C., Gleadle, J. M., McNeill, L. A., Hewitson, K. S., O'Rourke, J., Mole, D. R., Mukherji, M., Metzén, E., Wilson, M. I., Dhanda, A., *et al.* (2001) *Cell* **107**, 43–54.
- Bruick, R. K. & McKnight, S. L. (2001) *Science* **294**, 1337–1340.
- Jiang, B. H., Rue, E., Wang, G. L., Roe, R. & Semenza, G. L. (1996) *J. Biol. Chem.* **271**, 17771–17778.
- Arany, Z., Huang, L. E., Eckner, R., Bhattacharya, S., Jiang, C., Goldberg, M. A., Bunn, H. F. & Livingston, D. M. (1996) *Proc. Natl. Acad. Sci. USA* **93**, 12969–12973.
- Ebert, B. L. & Bunn, H. F. (1998) *Mol. Cell Biol.* **18**, 4089–4096.
- Kallio, P. J., Okamoto, K., O'Brien, S., Carrero, P., Makino, Y., Tanaka, H. & Poellinger, L. (1998) *EMBO J.* **17**, 6573–6586.
- Ema, M., Hirota, K., Mimura, J., Abe, H., Yodoi, J., Sogawa, K., Poellinger, L. & Fujii-Kuriyama, Y. (1999) *EMBO J.* **18**, 1905–1914.
- Carrero, P., Okamoto, K., Coumilleau, P., O'Brien, S., Tanaka, H. & Poellinger, L. (2000) *Mol. Cell Biol.* **20**, 402–415.
- Kung, A. L., Wang, S., Klco, J. M., Kaelin, W. G. & Livingston, D. M. (2000) *Nat. Med.* **6**, 1335–1340.
- Vo, N. & Goodman, R. H. (2001) *J. Biol. Chem.* **276**, 13505–13508.
- Pugh, C. W., O'Rourke, J. F., Nagao, M., Gleadle, J. M. & Ratcliffe, P. J. (1997) *J. Biol. Chem.* **272**, 11205–11214.
- Jiang, B. H., Zheng, J. Z., Leung, S. W., Roe, R. & Semenza, G. L. (1997) *J. Biol. Chem.* **272**, 19253–19260.
- Grossman, S. R., Perez, M., Kung, A. L., Joseph, M., Mansur, C., Xiao, Z. X., Kumar, S., Howley, P. M. & Livingston, D. M. (1998) *Mol. Cell* **2**, 405–415.
- Grossman, S. R. (2001) *Eur. J. Biochem.* **268**, 2773–2778.
- Mahon, P. C., Hirota, K. & Semenza, G. L. (2001) *Genes Dev.* **15**, 2675–2686.
- O'Rourke, J. F., Tian, Y. M., Ratcliffe, P. J. & Pugh, C. W. (1999) *J. Biol. Chem.* **274**, 2060–2071.
- Gu, J., Milligan, J. & Huang, L. E. (2001) *J. Biol. Chem.* **276**, 3550–3554.
- Lando, D., Peet, D. J., Whelan, D. A., Gorman, J. J. & Whitelaw, M. L. (2002) *Science* **295**, 858–861.
- De Guzman, R. N., Liu, H. Y., Martinez-Yamout, M., Dyson, H. J. & Wright, P. E. (2000) *J. Mol. Biol.* **303**, 243–253.
- Lin, C. H., Hare, B. J., Wagner, G., Harrison, S. C., Maniatis, T. & Fraenkel, E. (2001) *Mol. Cell* **8**, 581–590.
- Radhakrishnan, I., Perez-Alvarado, G. C., Parker, D., Dyson, H. J., Montminy, M. R. & Wright, P. E. (1997) *Cell* **91**, 741–752.
- Neri, D., Szyperski, T., Otting, G., Senn, H. & Wuthrich, K. (1989) *Biochemistry* **28**, 7510–7516.
- Matsuo, H., Li, H., McGuire, A. M., Fletcher, C. M., Gingras, A. C., Sonenberg, N. & Wagner, G. (1997) *Nat. Struct. Biol.* **4**, 717–724.
- Guntert, P., Dotsch, V., Wider, G. & Wuthrich, K. (1992) *J. Biomol. NMR* **2**, 619–629.
- Bartels, C., Xia, T., Billeter, M., Guntert, P. & Wuthrich, K. (1995) *J. Biomol. NMR* **6**, 1–10.
- Cornilescu, G., Delaglio, F. & Bax, A. (1999) *J. Biomol. NMR* **13**, 289–302.
- Brunger, A. T. (1992) in *A System for X-Ray Crystallography and NMR, Version 3.1* (Yale Univ. Press, New Haven, CT).
- Hoffman, R. C., Xu, R. X., Klevit, R. E. & Herriott, J. R. (1993) *J. Magn. Reson. Ser. B* **102**, 61–72.
- Conte, L. L., Chothia, C. & Janin, J. (1999) *J. Mol. Biol.* **285**, 2177–2198.
- Wang, Q. P., VanDusen, W. J., Petroski, C. J., Garsky, V. M., Stern, A. M. & Friedman, P. A. (1991) *J. Biol. Chem.* **266**, 14004–14010.
- Huber, A. H. & Weis, W. I. (2001) *Cell* **105**, 391–402.
- Dyson, H. J. & Wright, P. E. (2002) *Curr. Opin. Struct. Biol.* **12**, 54–60.
- Demarest, S. J., Martinez-Yamout, M., Chung, J., Chen, H., Xu, W., Dyson, H. J., Evans, R. M. & Wright, P. E. (2002) *Nature (London)* **415**, 549–553.
- Koradi, R., Billeter, M. & Wuthrich, K. (1996) *J. Mol. Graph.* **14**, 51–32.
- Kraulis, P. J. (1991) *J. Appl. Crystallogr.* **24**, 946–950.
- Nicholls, A., Sharp, K. A. & Honig, B. (1992) *Proteins* **11**, 281–296.
- Laskowski, R. A., Rullmann, J. A., MacArthur, M. W., Kaptein, R. & Thornton, J. M. (1996) *J. Biomol. NMR* **8**, 477–486.